Combined analysis methods for investigating titanium and nickel surface contamination after plasma deep etching

Rim Ettouri, Thomas Tillocher, Philippe Lefaucheux, Bertrand Boutaud, Vincent Fernandez, Neal Fairley, Christophe Cardinaud, Aurélie Girard, Rémi Dussart

Received: 10 June 2021 | Revised: 11 October 2021 | Accepted: 14 October 2021

DOI: xxx/xxxx

ARTICLE TYPE

Combined analysis methods for investigating titanium and nickel surface contamination after plasma deep etching

Rim Ettouri*[1,2] | Thomas Tillocher[1] | Philippe Lefaucheux[1] | Bertrand Boutaud[2] | Vincent Fernandez[3] | Neal Fairley[4] | Christophe Cardinaud[3] | Aurélie Girard[3] | Rémi Dussart[1]

[1]Groupe de recherches sur l'énergétique des milieux ionisés (GREMI), CNRS-University of Orléans, 14 rue d'Issoudun, BP 6744, F-45067 Orléans Cedex 2, France

[2]MISTIC SAS, 75 Promenade du Verger, 92130 Issy-les-Moulineaux, France

[3]Institut des matériaux Jean-Rouxel (IMN), CNRS-University of Nantes, 2 rue de la Houssinière, BP 32229, F-44322 Nantes Cedex 3, France

[4]Casa Software Ltd, Bay House, 5 Grosvenor Terrace, Teignmouth, Devon TQ14 8NE, UK

Correspondence
*Rim Ettouri. Email: rim.ettouri@univ-orleans.fr

Present Address
GREMI, CNRS-University of Orléans, 14 rue d'Issoudun, F-45067 Orléans, France

Abstract

Plasma etching techniques can result in damage and contamination of materials which, if not removed, can interfere with further processing. Therefore, characterisation of the etched surface is necessary to understand the basic mechanisms involved in the etching process, and enable process control and cleaning procedures to be developed. A detailed investigation by means of the combined use of Scanning Electron Microscopy coupled with Energy Dispersive X-ray Spectrometry (SEM/EDS), X-ray Photoelectron Spectroscopy (XPS) and Optical Microscopy (OM), has been carried out on deep titanium trenches etched by plasma. This innovative approach has provided a further insight into the microchemical structure of the surface contamination layer on both the titanium and the nickel hard mask surfaces. The described experiments were conducted on 25 to 100μm wide trenches, first etched in bulk titanium by an optimised $Cl_2/SF_6/O_2$-based inductively coupled plasma process, through an electroplated nickel hard mask. The results allow to identify chlorine, fluorine, and carbon as the main contaminating agents of the nickel mask, and to associate three oxidation states around the etched trenches highlighting certain specific aspects related to the passivation mechanism. These observations reinforce the scientific relevance of the combined use of complementary optical and imaging analytical techniques.

KEYWORDS:
Titanium, X-ray Photoelectron Spectroscopy (XPS), Scanning Electron Microscopy (SEM), Energy Dispersive X-ray Spectroscopy (EDS), imaging, X-ray Photoelectron Spectroscopy Imaging (XPSI)

1 | INTRODUCTION

The etching of deep structures with a high aspect ratio is a critical technological step in the realisation of MEMS. The dry etching of titanium (Ti), amongst other unconventional materials, requires the development of specific and yet incompletely understood etching processes. Fluorinated, but especially chlorinated chemistries appear in the literature reporting deep plasma etching of Ti[? ?]. In 2004, Aimi et al. developed the MARIO (Metal Anisotropic Reactive Ion etching with Oxidation) process[?] which consists in alternating short Cl_2/Ar etching plasmas with short pure O_2 plasmas in an Inductively Coupled Plasma - Reactive Ion Etching (ICP-RIE) system. The oxygen plasma steps allow the sidewalls of the etched titanium structures to be oxidised and thus limit lateral etching, which leads to anisotropic profiles with scalloping. A year later, Parker et al. developed and patented a second technique for the deep etching of titanium, called Titanium ICP Deep Etch process (TIDE)[? ? ?], which uses only a continuous Cl_2/Ar plasma. The etch rate is much higher than that of the previous method, 2.2μm.min^{-1} instead of 0.5μm.min^{-1}, and the process allows

vertical sidewalls to be obtained without scalloping. Furthermore, the Alternated Process for the deep Etching of Titanium (APETi) developed at the GREMI laboratory in 2013 by Tillocher *et al.*on an ICP reactor, alternating a Cl_2/Ar plasma and an SF_6 plasma, has shown its ability to deep etch titanium effectively by reducing the roughness at the etch front as well as improving the reproducibility[?,?]. A plasma combining both chlorine and fluorine chemistries has been reported in the literature to efficiently etch titanium[?]. When those two chemistries are used separately, it is shown that the first chlorination is endothermic for one case and the fluorinated etch product has a low volatility in the second case, which limits titanium etching. However, if they are combined, they act in synergy to etch efficiently titanium by producing an fluoro-chloride intermediate product which skips the first endothermic chlorination and leads to a volatile chlorine containing etch product. More specifically, the benefit of combining chlorine plasmas with sulphur hexafluoride (SF_6) on titanium etching was confirmed by Laudrel *et al.*[?]. Although it has been shown that high etching rates have been reached with very good profiles in chlorine and mixed chemistries, the analysis of remaining species on the surface after etching is not yet well documented. However, it is crucial to study the surface composition after the plasma process to better understand the etching mechanisms and analyse the residual by-products remaining at the surface after etching. This is all the more important as the previously mentioned etching processes enable the fabrication of titanium-based microsystems for biomedical applications such as vascular stents [?,?], micro-needles for drug delivery [?,?,?] or biosensors[?]. It is therefore necessary to characterise the contamination at each step of the microfabrication process, including after etching, to keep the device biocompatible and the contaminants below the tolerated levels. For instance, pure grade 1 titanium must contain the lowest levels of oxygen ($O \leq 0.18\,\%$ by weight), hydrogen ($H \leq 0.015$ wt.%) and iron ($Fe \leq 0.25$ wt.%), producing the most ductile of the four commercially pure grades[?]. Surface investigation can be achieved by selecting the appropriate diagnostic techniques. On the one hand, Scanning Electron Microscopy (SEM) combined with Energy-Dispersive X-ray Spectroscopy (EDS) microanalysis was proven as an efficient routine method for determining surface chemistry and how this chemistry changes at the surface and in the surroundings of the etched patterns. On the other hand, space resolved X-ray Photoelectron Spectroscopy (XPS) has evolved into a versatile analytical tool extremely useful, suitable for the complete and quantitative characterisation of the elemental composition and the state of the chemical bonds on the surface of materials. Our work below shows how a multi-technique approach, using SEM/EDS analysis, XPS combined with imaging and optical microscopy, provides quantitative elementary and chemical information with extremely high surface specificity on residual species on the mask and etched titanium patterns.

2 | EXPERIMENTAL SECTION

2.1 | Sample preparation

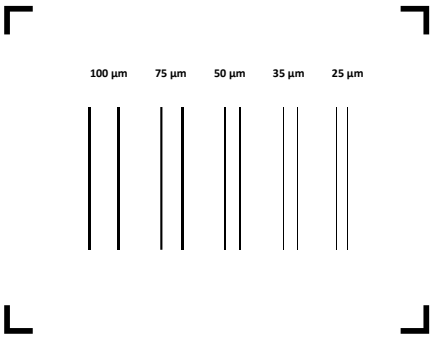

FIGURE 1 Drawing of a single cell pattern repeated 22 times on the 4" photomask

A commercially pure grade 1 titanium wafer, with a 4-inch diameter and a thickness of $300\,\mu\mathrm{m}$, was used to prepare the samples. First, the substrate was patterned by standard photolithography process and a 3 μm-thick nickel hard mask was electroplated. Then, $13 \times 16.5\,\mathrm{mm}^2$ samples, each containing 25 to $100\,\mu\mathrm{m}$ wide and $5\,\mathrm{mm}$ long trenches were cut with a wire saw (Fig. 1). The samples were glued with vacuum grease to a 4" titanium wafer completely covered with electroplated nickel, so that no additional material was introduced into the reactor chamber. After a 45 minutes long $Cl_2/SF_6/O_2$ etching process in the ICP reactor, the samples were first characterised using optical microscopy (OM). They were transported in air to the digital microscope, which is located in the same clean room as the etching reactor. The image assemblies of the different trenches on the etched sample took approximately 15 minutes. The sample was then introduced into the SEM chamber (at a pressure of approximately 10^{-6} mbar) and a first chemical analysis of the surface was performed by SEM/EDS-mapping images which took approximately 45 minutes. Finally, to prevent any further contamination by air exposure, the samples were placed under vacuum and transported to the XPS chamber where they were analysed within five days.

2.2 | Instrumentation

2.2.1 | Scanning electron microscopy with energy dispersive spectroscopy

The investigations were conducted with a Zeiss SUPRA 40 field emission scanning electron microscope operated at $10\,\mathrm{keV}$ accelerating voltage and a working distance of $9\,\mathrm{mm}$ employing a secondary electron (SE2; Everhart-Thornley) detector. The elemental composition was obtained using a Bruker Quantax EDS detector. Samples were mounted on SEM stubs secured by conductive clips, which eliminates contamination issues due to adhesives or glues.

2.2.2 | X-ray photoelectron spectroscopy

XPS measurements were performed using a Kratos Axis Nova X-ray photoelectron spectrometer with a monochromatic Al Kα X-ray source operated at 15 kV and 20 mA. No charge neutralisation has been used during data acquisition. The spectra were collected using the combination of electrostatic and magnetic lenses for large area acquisition (700 $\mu\mathrm{m} \times 300\ \mu\mathrm{m}$). Survey and high-resolution scans were acquired at pass energies of 80 and 40 eV, corresponding to an all over Fermi edge resolution of 0.95 and 0.55 eV with 0.5 and 0.1 eV step intervals, respectively. The samples were exposed to X-rays for approximately 12 hours. In the case of patterned samples, these were oriented in azimuth so that the trenches are parallel to the projection of the X-ray beam on the surface. Thus, the X-rays could irradiate the trench down to its bottom. Indeed, in reason of the trench geometry (depth 80 $\mu\mathrm{m}$, width 100 $\mu\mathrm{m}$) and the value of the attenuation length in Ti for 1487 eV X-rays[?], any other orientation would not allow to observe the trench bottom. Photoelectron images of 256×256 pixels were acquired using the pass energy of 40 eV and a Ag 3d5/2 resolution of 1 eV over the field of view of 450 $\mu\mathrm{m}$ by 450 $\mu\mathrm{m}$. All data analyses were carried out using CasaXPS software[?]. Whenever spectra treatment was achieved, we used a Tougaard U2 background and LF spectral shapes.

3 | RESULTS AND DISCUSSION

3.1 | Preliminary screening by optical microscopy

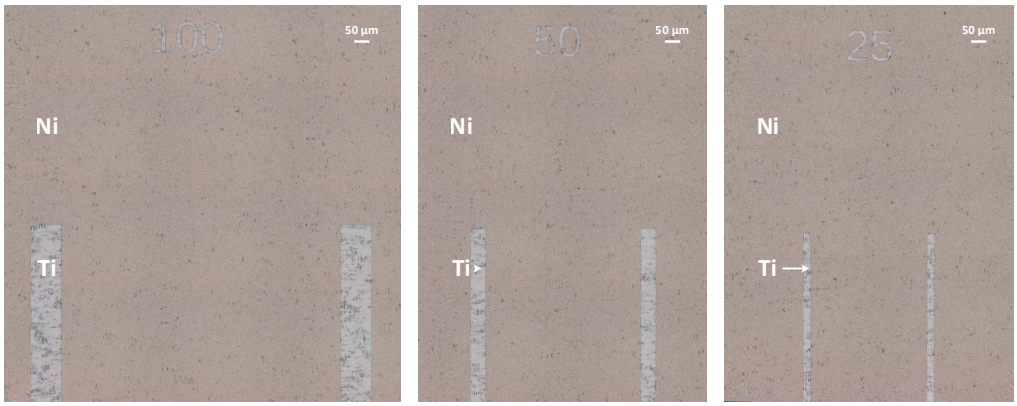

FIGURE 2 Top view images of the wafer surface showing trenches of different widths before etching: 100 $\mu\mathrm{m}$ (left), 50 $\mu\mathrm{m}$ (middle) and 25 $\mu\mathrm{m}$ (right) wide trenches

OM investigations were performed using a Keyence VHX-5000 digital microscope with a 500x objective. Fig. 2 shows optical images of the mask areas surrounding the trenches: the 5 mm-long trenches correspond to bulk titanium and the rest of the surface is covered by nickel.

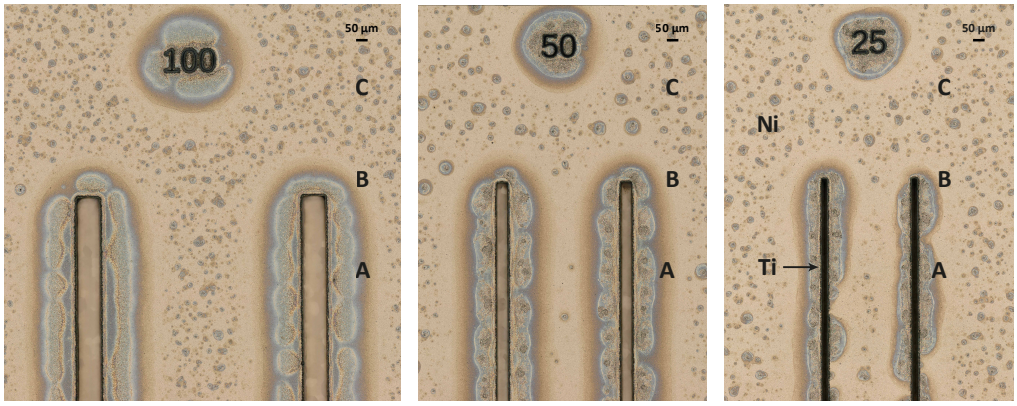

FIGURE 3 Top view images of the wafer surface showing trenches of different widths after etching: 100 $\mu\mathrm{m}$ (left), 50 $\mu\mathrm{m}$ (middle) and 25 $\mu\mathrm{m}$ (right) wide trenches

The first observations after etching revealed the presence of residues as well as a coloration of the mask around the trenches. Three clearly identifiable zones can be observed: a first grey area (designated by the letter A in Fig. 3), with a pale blue contour, can be discerned at the periphery of the trenches whatever the widths; an intermediate zone (designated by the letter B) of a few tens of microns, without spots, which seems to closely match the shape of the first one; and a large area (designated by the letter C) of the mask covered with grey spots that seem to have different diameters.

3.2 | Structure, morphology and EDS microanalysis of the materials deposited on the mask surface

The surface of the samples was characterised by SEM/EDS before and after plasma etching. The composition of the surface in a non-etched reference sample was determined using EDS analysis, both on the Ni mask (Fig. 4a in blue) and in the trench (Fig. 4b in green). The EDS spectrum before etching, displayed in Fig. 4a, shows that, in addition to Ni and O due to spontaneous oxidation with ambient air in clean room, an additional peak of C is present. Similarly, as shown in Fig. 4b, peaks of Ti, O and C are detected along the trench. It should be noted that this analytical technique allows the determination of the elemental composition at a point, along a line, or in a defined area with a high degree of precision. Furthermore, the electrons penetrate from the surface to an estimated depth of 1 μm into the sample[?], which explains why no titanium lines appear in the spectrum corresponding to the mask which initially had a thickness of 3 μm.

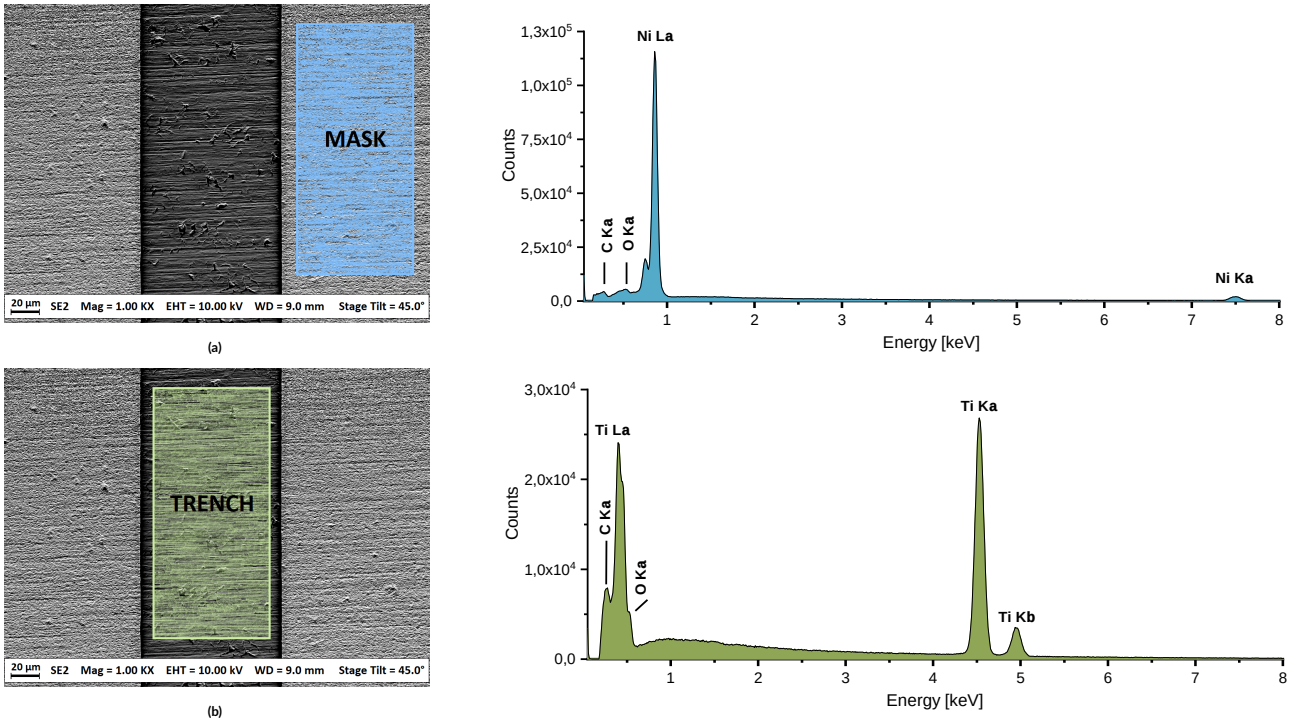

FIGURE 4 SEM images of a 100 μm wide trench before etching and EDS spectrum of (a) the electroplated Ni mask and (b) titanium

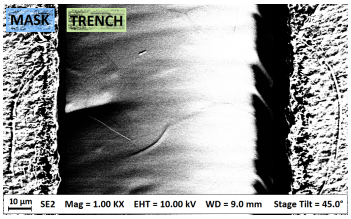

FIGURE 5 A top view SEM image of a 100 μm wide trench after etching

Figure 5 shows an SEM image of both the Ni mask and a 100 μm wide trench after a 45-minute $Cl_2/SF_6/O_2$-based inductively coupled plasma reactive ion etching (ICP-RIE) process. The sample is tilted by 45°, such that the area of interest is oriented normal to the EDS detector. It should be noted that the trench is about 80 μm deep, which is the reason for the strong shadow effect on the right side of the mask. The surface structure of the mask seems to have changed, giving way to an apparent roughness. This surface morphology is induced by the strong ion bombardment during the etching step.

TABLE 1 The concentration of major elements in weight percentage (Wt.%) and atomic percentage (At.%)

Element	Ni (%)	Ti (%)	C (%)	O (%)	F (%)	Cl (%)
Wt. (%)	1.01	86.77	3.88	4.30	1.28	0.02
At. (%)	0.68	72.15	12.86	10.69	2.68	0.02
Error (%)	±0.15	±2.92	±0.45	±0.50	±0.18	±0.00

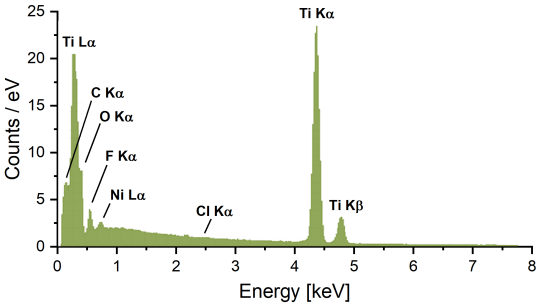

FIGURE 6 EDS spectrum of the titanium trench after etching

Table 1 gives the elemental composition of the titanium trench surface in weight percentage (Wt.%) and atomic percentage (At.%) extracted from the EDS spectrum displayed in Fig. 6. These values should be treated as guides only as they are based on Standardless PB/ZAF quantitative elemental analysis performed using the Bruker ESPRIT software. Besides the elements already detected before etching, a very low concentration of Cl and Ni is detected in the trench, which is consistent with the fact that no micromasking is noted during this etching. However, it is perfectly normal to detect fluorine on both the mask and the substrate, as the formed etch-products (NiF_2/NiF_3, TiF_3/TiF_4) are not volatile at the temperatures reached during the plasma etching.

Figure 7 displays the EDS cartography of the sample. More precisely, Fig. 7a is the corresponding SEM image and Figs. 7b–7f display the mapping of Ti, Ni, F, C, O, and Cl elements, respectively. These mappings show the spatial distribution of the elements on the surface. The total map acquisition time was approximately 15 minutes. It appears that the concentration of oxygen is higher at the extreme periphery of the trench than on the rest of the mask. Furthermore, the distribution of chlorine seems to be complementary to that of oxygen, since its concentration is lower at the edge of the trench. The other elements exhibit no particular behaviour. As expected, titanium is located inside the trench and nickel outside. Both C and F are present everywhere at the sample surface.

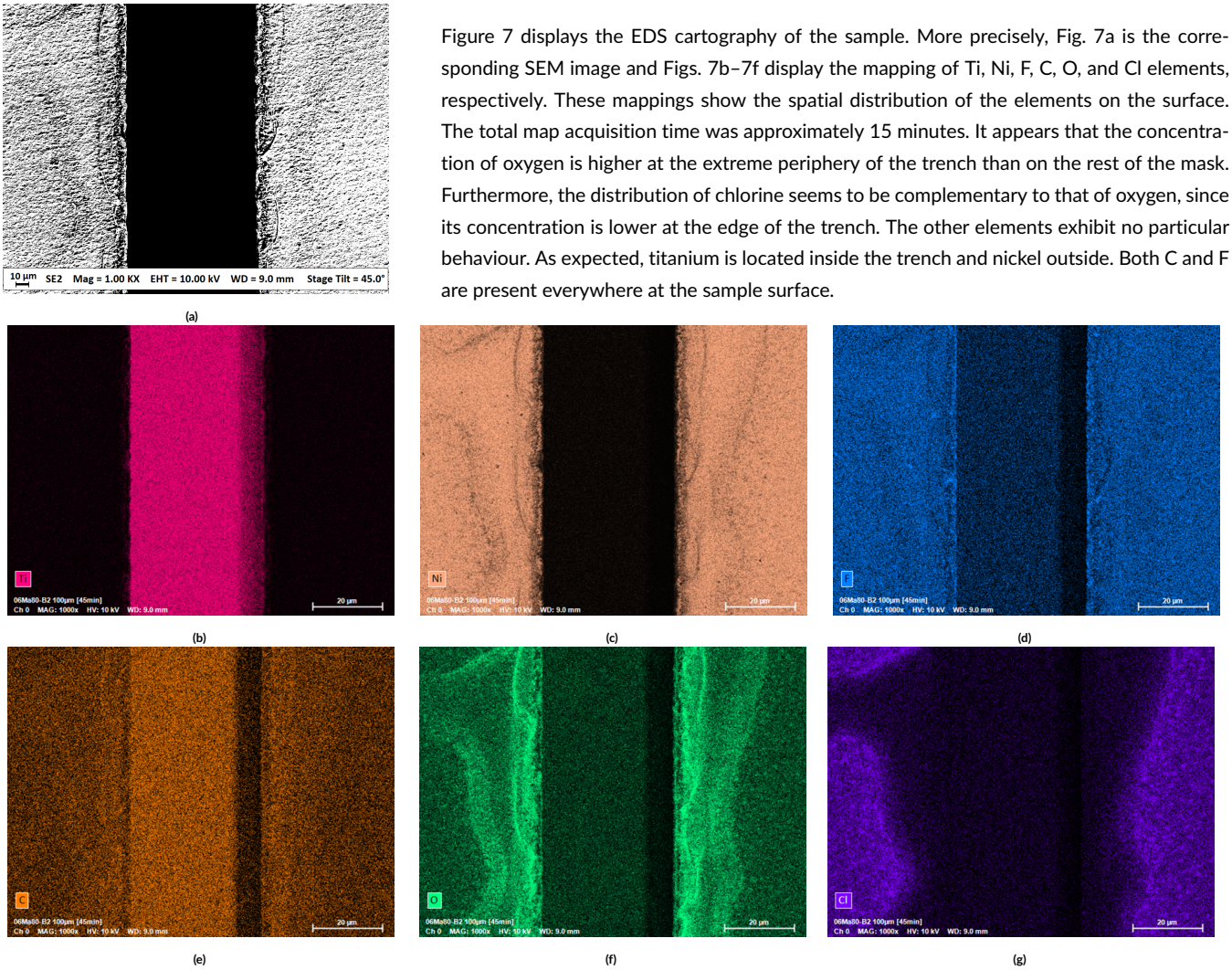

FIGURE 7 EDS cartography showing a mapping of Ti, Ni, F, C, O, and Cl elements on the etched sample

3.3 | X-Ray Photoelectron Spectroscopy analysis

3.3.1 | Component analysis of the Ni mask and Ti surface before etching

Figure 8a shows a wide XPS scan of the surface of the Ni mask. The analysis before etching was performed on a sample from the same wafer, which was not exposed to plasma. The results before etching are in good agreement with EDS data. Initially, the electroplated mask was found to contain Ni, signature for carbon and oxygen as surface contamination are also observed. Figures 8b and 8c show the Ni 2p and O 1s spectra collected for the electrodeposited Ni surface. The Ni 2p spectrum presents the contributions from metallic Ni and $Ni(OH)_2$ (Ni 2p3/2 at 852.4 eV with a FWHM of 0.88 eV and 856.1 eV a FWHM of 2.61 eV respectively) and from the plasmon loss and shake up satellites, while the analysis of the O 1s spectrum shows an O^{2-} contribution from the $Ni-O$ at 529.5 eV with a FWHM of 0.96 eV. Therefore, a NiO component must also be considered; however, its position at 853.7 eV [?] makes it difficult to locate. The main O 1s structure can be fitted with four components, $(H)O-Ni$ at 531.6 eV with a FWHM of 1.50 eV, and surface contamination species due to exposure to the ambient air is responsible for the other O 1s components: OH (adsorbed water and carbonyl) at 533.4 eV with a FWHM of 1.50 eV, $O-C$ at 532.5 eV with a FWHM of 1.38 eV and $O=C$ at 530.9 eV with a FWHM of 1.38 eV. Accordingly, the C 1s species shown in Fig. 8d correspond to $C-C$, $C-H$ (285.0 eV, FWHM of 1.35 eV), $C-O$ (286.4 eV, FWHM of 1.73 eV), $C=O$ (287.4 eV, FWHM of 1.73 eV) and COOH (288.7 eV, FWHM of 1.54 eV).

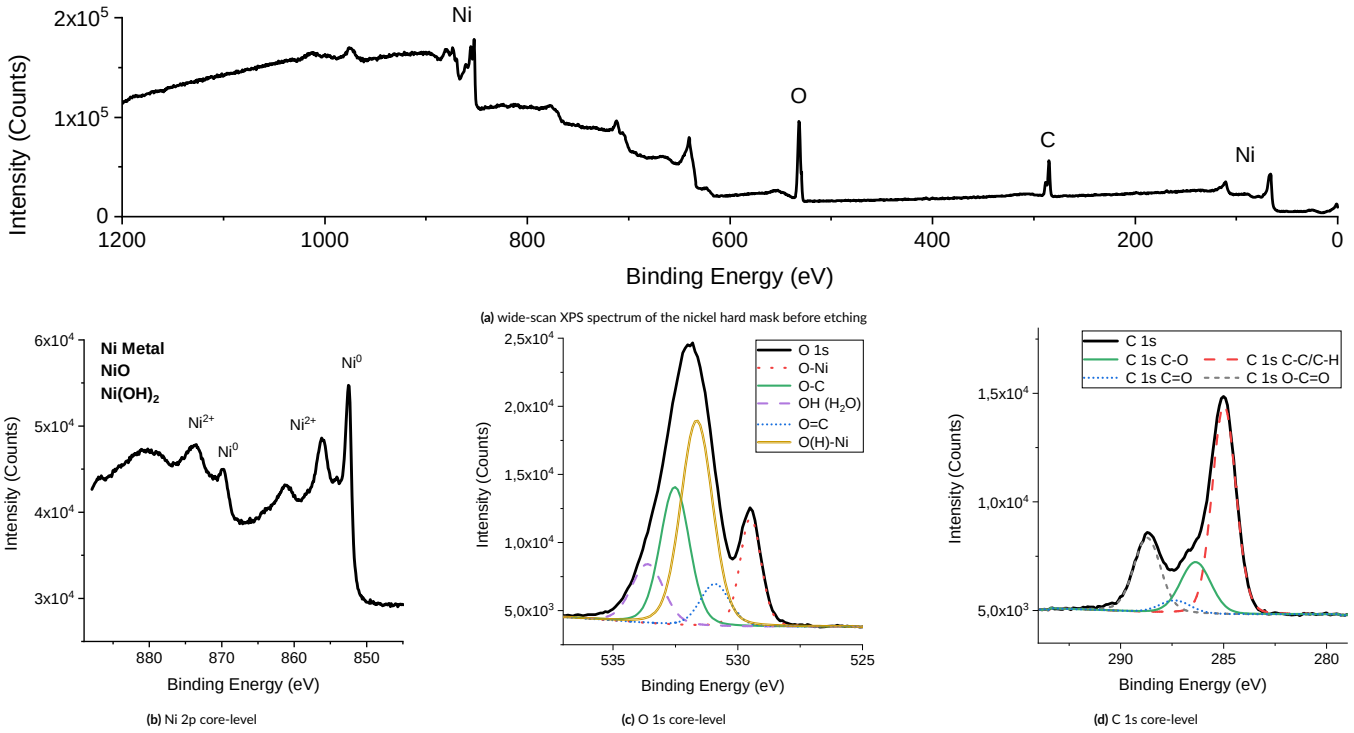

FIGURE 8 XPS spectra of the nickel hard mask before etching: (a) survey scan, (b) Ni 2p, (c) O 1s, and (d) C 1s

These XPS measurements indicate that the electrodeposited nickel is hydroxidised, which is certainly a consequence of electrodeposition from an aqueous solution (Watts nickel bath).

The XPS survey scan of the Ti surface before etching illustrates the presence of Ti, O, C as well as traces of Fe and N, which corresponds to the characteristics of grade 1 titanium ($N \leq 0.03,\ C \leq 0.08,\ H \leq 0.01,\ Fe \leq 0.20$and $O\ \leq 0.18$Wt.%). High resolution spectra of the Ti 2p, O 1s and C 1s core levels are shown in Fig. 9.

The Ti 2p spectrum presents a weak Ti^0 contribution (Ti 2p3/2 at 454.1 eV) and an intense Ti^{2+} contribution (Ti 2p3/2 at 458.7 eV), the latter being characteristic of TiO_2. The results show that the Ti surface is initially oxidised. It is indeed common knowledge that, when titanium is exposed to air or water, it spontaneously forms native titanium dioxide. In agreement, the O 1s spectrum shows an intense contribution at 530.1 eV attributed to $O-Ti$ groups. All other contributions in the O 1s and the C 1s spectra come from the carbonaceous surface contamination, except for the C 1s contribution at 281.7 eV that can be attributed to $C-Ti$ groups. Contribution of these species to the Ti 2p spectrum should fall around 454.7 eV (Ti 2p3/2) [??], apparently it is too weak to be observed.

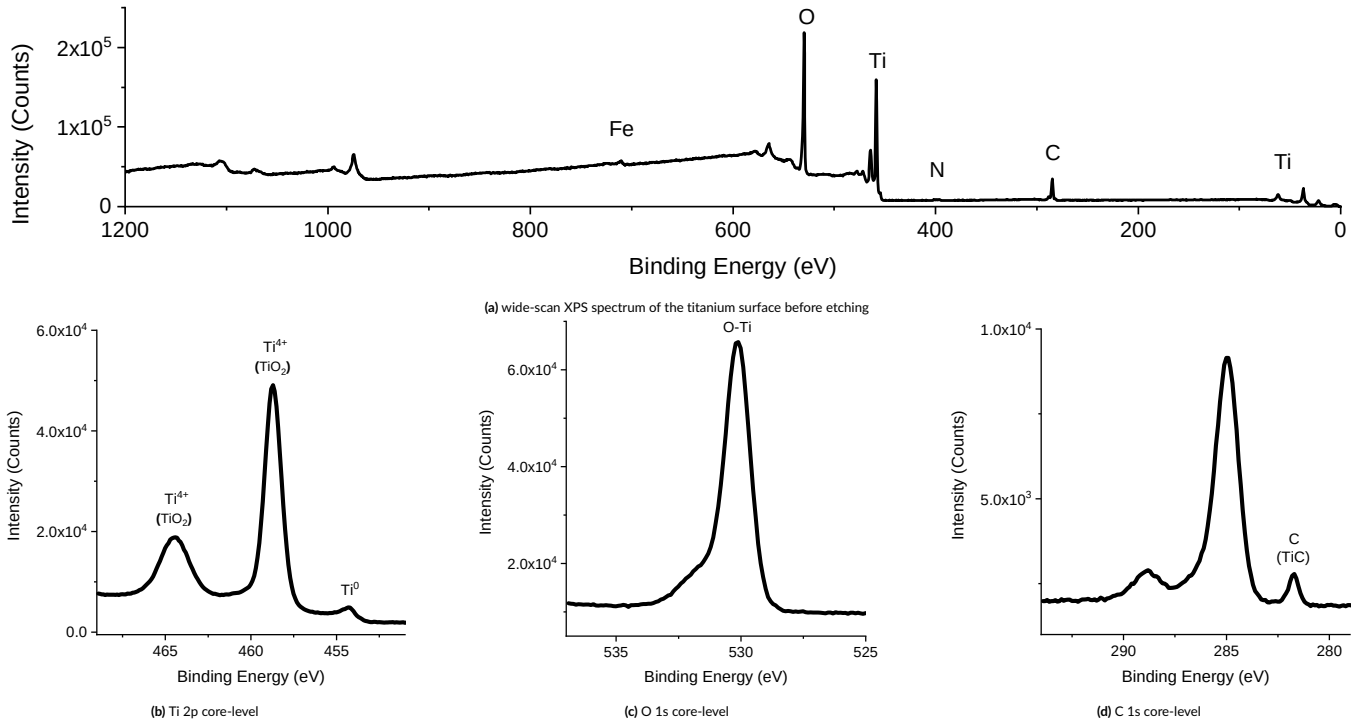

FIGURE 9 Wide-scan XPS spectrum of the titanium surface and high-resolution XPS spectra of (b) Ti 2p, (c) O 1s and (d) C 1s for the sample before etching

3.3.2 | Component analysis of the Ni surface after etching

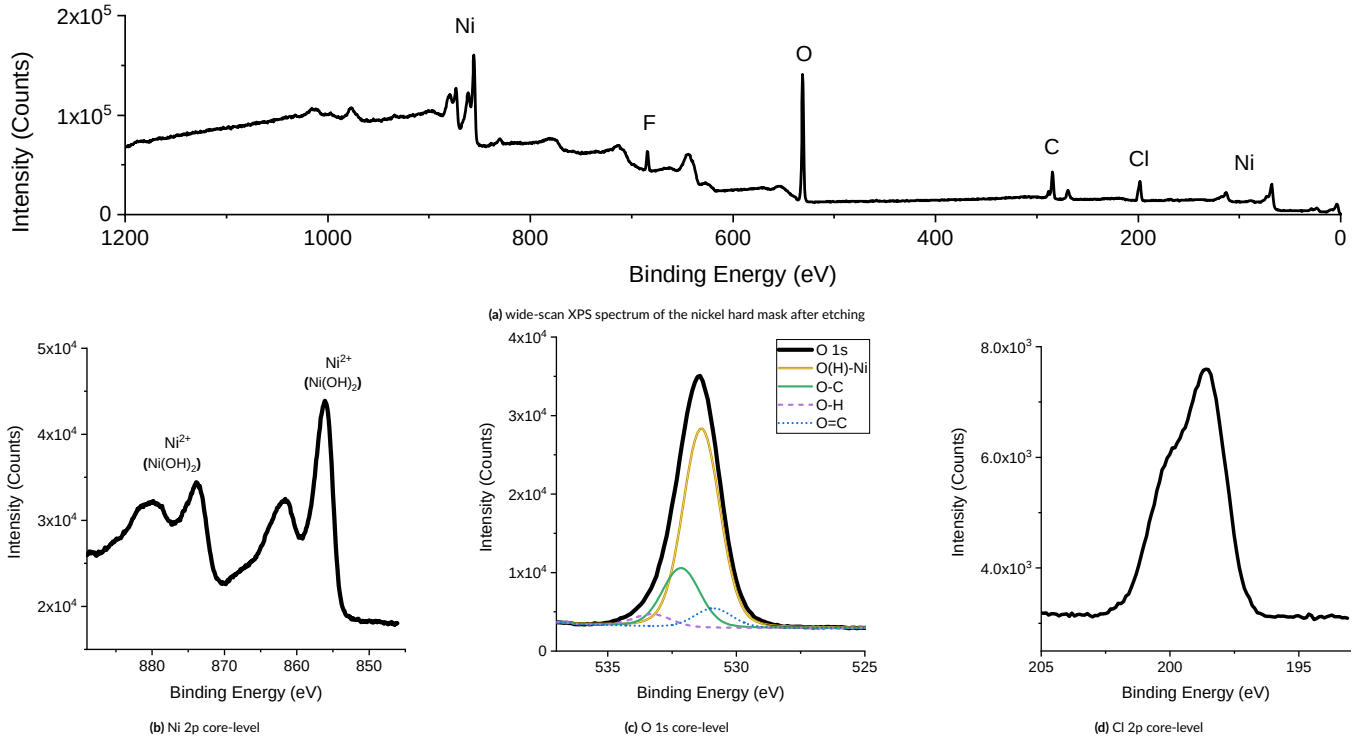

FIGURE 10 XPS spectra of the nickel hard mask after etching: (a) survey scan, (b) Ni 2p, (c) O 1s, and (d) Cl 2p

The survey XPS spectrum of the Ni surface after etching, displayed in Fig. 10a, confirms the existence of Ni, O, C, F and Cl elements at the mask surface after etching, which is consistent with the EDS mapping result shown previously. However, Fig. 10b shows that the metallic Ni peak disappears after etching. The main peak at 856.0 eV is compatible with a mixture of $Ni(OH)_2$ (856.1 eV) and $NiCl_2$ (855.8 eV) groups. However, the former appears to be more probable when considering the overall shape of the spectrum and reference data for $Ni(OH)_2$ and $NiCl_2$[?]. In agreement, the O 1s spectrum shows an intense contribution at that can be related to $(H)O-Ni$ species, and presents $O(C)$s and OH features as well (Fig. 10c). The other features in the Ni 2p spectrum at 861.7 and 866.8 eV correspond well to the satellites in $Ni(OH)_2$. The Cl 2p spectrum shows a unique doublet, which attribution is difficult (Fig. 10d) but XPS imaging (Section 3.4) will provide additional insight. The F 1s spectrum (not shown) does not show particular features, its position at 684.7 eV can correspond to $F-Ni$ groups; these, expected at 858 eV[?] are not distinguished on the Ni spectrum. As for the C is spectrum (not shown), it presents only surface contamination related contributions. The overall quantification (Table 2) does not bring any conclusive information about the nature of the Cl and F related species.

TABLE 2 Quantification of the survey scan in atomic percentage (At.%)

Element	Ni (%)	Ti (%)	C (%)	O (%)	F (%)	Cl (%)
Ni hard mask before etching	28	–	36	36	–	–
Ti substrate before etching	–	26	21	53	–	–
Ni mask after etching	26	–	23	39	5	7
Ti etched pattern (Ni mask is present)	24	2	24	43	3	5

3.3.3 | Component analysis of a Ti etched pattern

The survey XPS spectrum of the sample surface containing a Ti etched trench is displayed in Fig. 11a. It shows Ti, Ni, O, C, F and Cl elements. It is worth noting that, despite the 100 $\mu\mathrm{m} \times 5\ \mathrm{mm}$ (width x length) area of the trench, the data collected by the detector (700 $\mu\mathrm{m} \times 300\ \mu\mathrm{m}$ analysed area) do not only correspond to the bottom of the trench but also to the surface of the surrounding mask. This explains the high intensity of nickel compared to titanium in Fig. 11. For O, C, F and Cl. The spectrum observed is thus the combination of that coming from the Ti trench, that from the Ni mask "far from the trench", as in the previous case, and that from the Ni mask "close to the trench". The latter two could present different chemical composition as suggested by the differences observed in EDS (Fig. 7) and optical (Fig. 3) imaging. This is put forward as the most probable reason for the change observed in the O 1s and Cl 2p spectra (Fig. 11b and Fig. 11c). In addition, it also appears that the F 1s and C 1s spectra (not shown) present a different shape suggesting changes in the C and F chemical environment.

The Ti 2p spectrum (Fig. 11d) does not show any contribution from metallic Ti (Ti^0). The Ti 2p3/2 is located at 458.7 eV, which is in good agreement with the TiO_2 contribution observed before etching. The spectroscopy analysis and interpretation of core-level spectra could not offer the possibility to analyse the selectively trench bottom as well as the mask at the vicinity of the trench opening. Therefore, to clarify the spatial distribution of the detected elements and their respective chemical environment, and to further develop the analyses previously carried out by EDS mapping, it is necessary to proceed with analyses by XPS imaging.

3.4 | X-Ray Photoelectron Spectroscopy imaging

3.4.1 | Data acquisition and pre-treatment

XPS imaging analysis can help to determine the chemical composition and distribution of the various chemical compounds on the surface of the mask, and thus extend previous EDS studies. This analytical technique is very powerful and offers the possibility of correlating chemistry on a microscopic scale with imaging. For this purpose, we acquired spectral image data sets on the sample, where each pixel of an image contains a spectrum. Therefore, to analyse such a large amount of data, it is necessary to use multivariate analysis techniques to reduce the dimensionality of the data, as there are too many spectra to interrogate individually. Photoelectron images of 256×256 pixels were acquired using the pass energy of 40 eV over the field of view of 450 $\mu\mathrm{m}$ by 450 $\mu\mathrm{m}$, with a spatial resolution lower than 8 $\mu\mathrm{m}$. First, the image size was reduced to 128×128 pixels, by summing the neighbouring pixels, in order to improve the signal-to-noise ratio by a factor of two. Amongst the multivariate analysis techniques, one of the most popular, is the Principal Component Analysis (PCA) which expresses the data using linearly uncorrelated orthogonal variables called principal components[? ? ?]. This technique reduces the dimensionality of a large data set by projecting it into a lower-dimensional orthogonal basis. Subsequently, data reconstruction based on these components alone results in a significant improvement in signal-to-noise ratio. Images were converted to spectra at each pixel. Linear backgrounds were then subtracted from each spectrum. The next step used in the XPS quantification

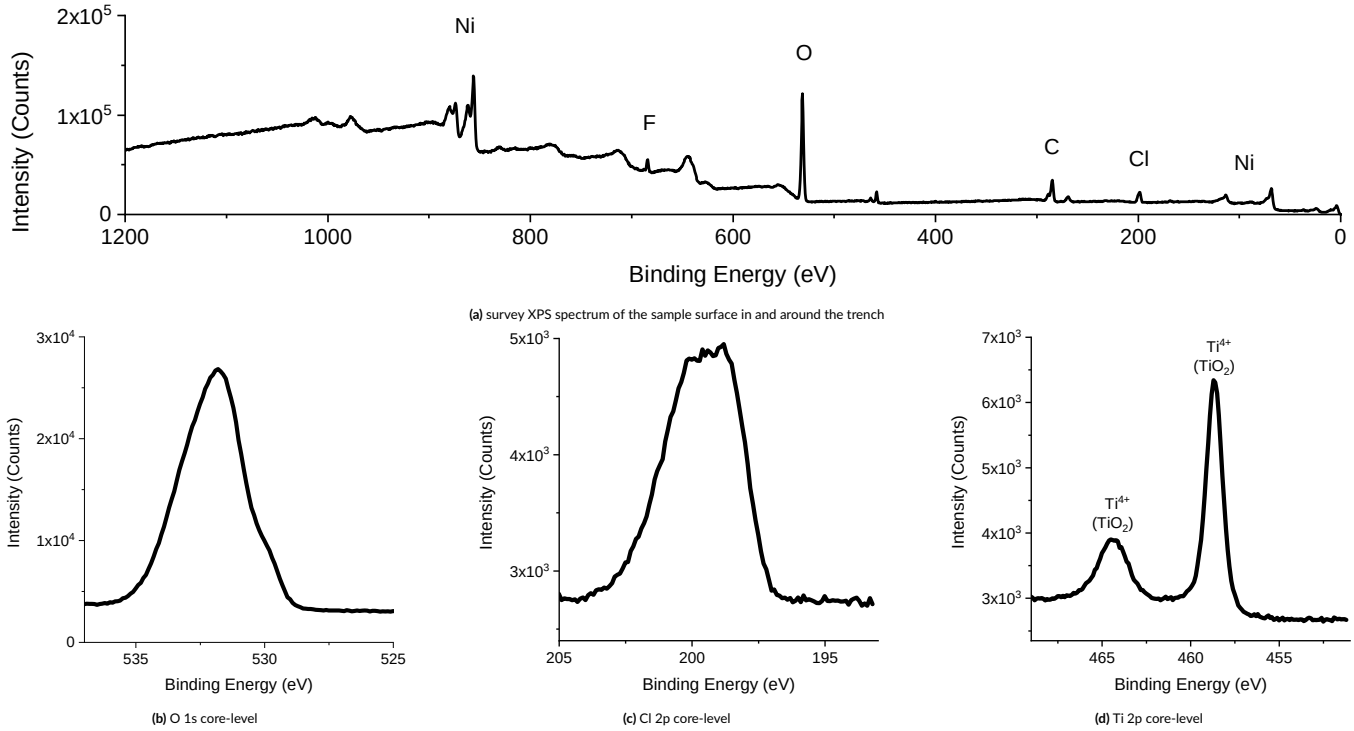

FIGURE 11 (a) Survey XPS spectrum of the titanium surface contamination after etching, (b) O 1s, (c) Cl 2p and (d) Ti 2p high-resolution XPS spectra after etching

process was to integrate the signal from the background subtracted intensity and then apply intensity corrections to provide representative images of the sample composition. The seven maps presented in Fig. 12 correspond respectively to the seven elements detected in the previous XPS spectra: Ni 2p, Ti 2p, C 1s, O 1s, F 1s, Cl 2p and N 1s.

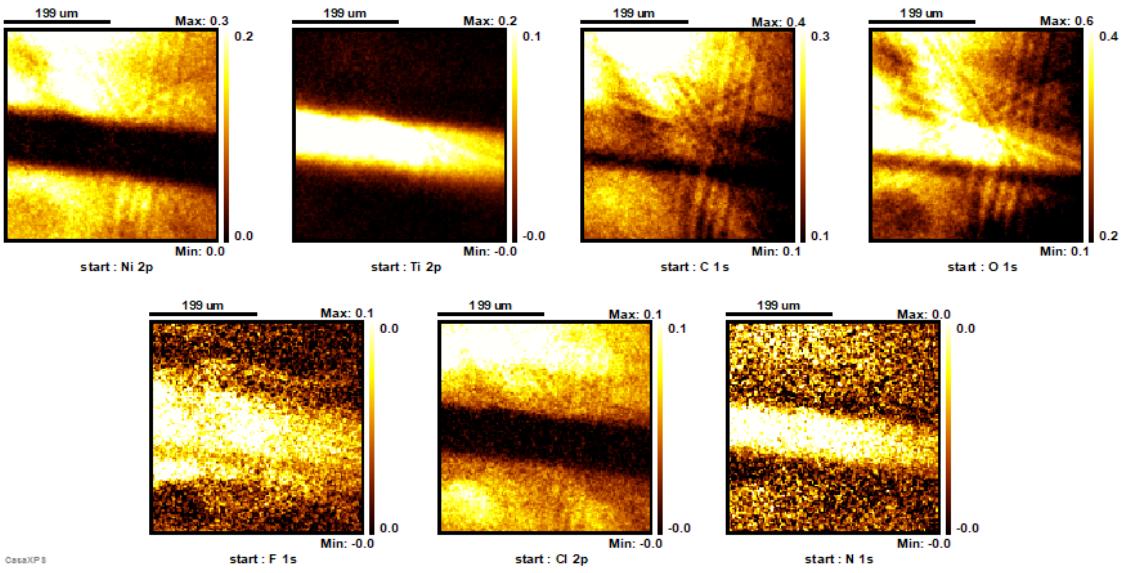

FIGURE 12 Intensity maps corresponding respectively to Ni 2p, Ti 2p, C 1s, O 1s, F 1s, Cl 2p and N 1s regions

3.4.2 | Quantitative XPS imaging

The data were then quantified using Scofield cross-sections[?] and effective attenuation length[?], resulting in chemical-state maps that reveal the spatial location of elements. There was no need for transmission function correction using this measurement mode. These quantitative region maps confirm the EDS results and give more precision about element chemical states. Figure 13 shows the Ti 2p map with a homogeneous distribution of titanium along the trench bottom, and the complementary Ni 2p map. The C 1s, O 1s, F 1s, Cl 2p and N 1s region maps all provide interesting information on the spatial distribution of the elements. For instance, there is a similarity in distribution between the Cl 2p and C 1s elements, and their presence is complementary to that of O 1s. In addition, the regions A and B of the mask at the periphery of the trench, as defined previously in the digital microscopy images (Fig. 3), are easily identified, which was not the case in the EDS cartography. We also notice spots with a high concentration of Cl, C and N. However, fluorine seems to be more present at the edge of the trench and a little bit at its bottom, probably due to redeposition of the etching products.

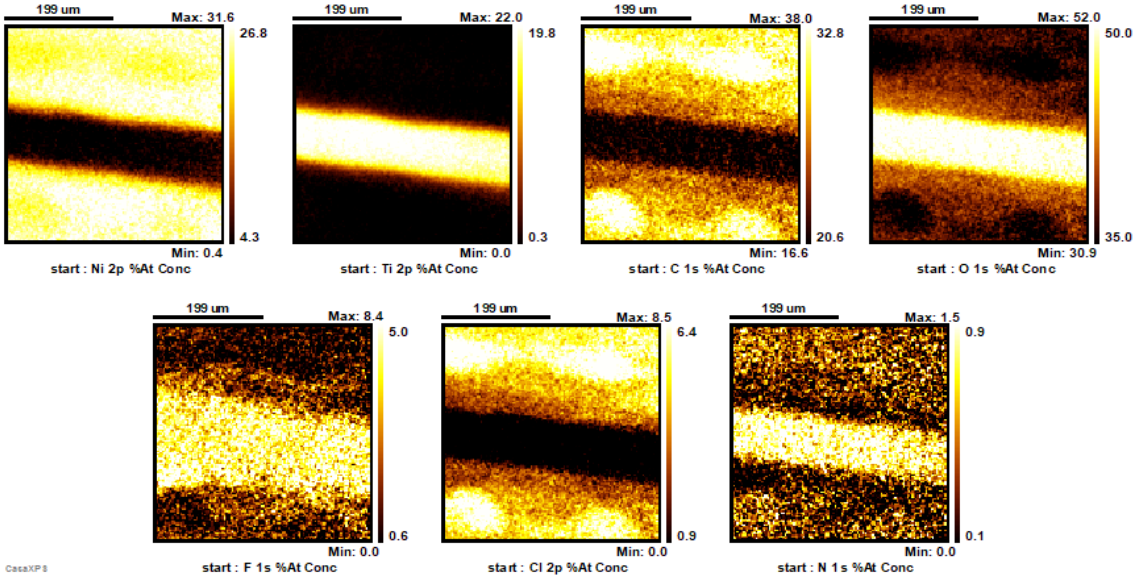

FIGURE 13 Quantitative regions maps corresponding to Ni 2p, Ti 2p, C 1s, O 1s, F 1s, Cl 2p and N 1s for etched samples

It is worth pointing out that individual images acquired at specific binding energies are, in fact, a combination of chemically significant electrons, scattered electrons and instrumentation errors. The quantification process of the image data aims to reduce the influence of both the measurement mechanism and background on the obtained quantification values. As such, when different chemical environments are suspected, the image measurements at the peak positions should be adjusted using the background images and normalised to the total image intensity to provide images representative of the sample composition. Information on chemical bonding can then often be obtained from the photoelectron emission spectra by noting the 'chemical shifts' in the energy positions of the XPS electrons.

Data smoothing in the spatial domain resulted in a slightly more homogeneous image, thus reducing the scale to the range 31.2-49.3 of atomic percentage concentration (%At Conc). The images in Fig. 15 are displayed using this reduced interval and the colour scale from Fig 14. More precisely, Figure 15a corresponds to O 1s region with an atomic concentration of less than 34.8%, Figure 15b to the region between 34.81% and 36.64%, Figure 15c to the region between 36.65% and 38.47%, Figure 15d to the region between 38.48% and 40.77%, Figure 15e to the region between 40.78% and 46.88%, and Figure 15f to the region of more than 46.89%. This approach provides the opportunity to perform appropriate quantification at each pixel of the image and thus obtain quantifiable results related to the spatial dimensions of the pixels in the image, for the features appeared following the etching.

The raw spectra at the pixels were summed to produce as many spectra of an image data set as there were false colours in the mask image. The procedure of summing spectra from similar pixels provides an independent approach for generating spectra from the raw data in image data sets with an acceptable signal-to-noise ratio for peak-fitting and quantification. Subsequently, six spectra were generated by summing the pixels corresponding to each of the false colours in the mask image (Fig. 16).

The processed spectra clearly show the shapes of three underlying peaks for O 1s. The presence of the O 1s at higher binding energies, $531.6\,\mathrm{eV}$, suggests the presence of hydroxyl ($-$OH) groups on the surface of the mask (contribution of Ni $-$ OH bonds)[?]. The presence of the peak at $533\,\mathrm{eV}$

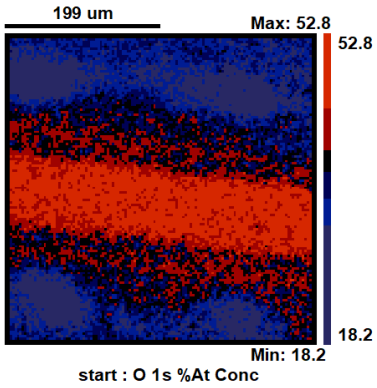

FIGURE 14 False colour scale highlighting the regions of interest

One of the regions of interest that particularly caught our attention was that corresponding to oxygen. The process of quantification in the case of oxygen goes through several steps and starts with processing a set of images acquired at regular energy steps, covering the full interval required to quantify the sample surface. The first step was to define a false-colour visualisation of an image, where various intensity ranges were assigned different pixel colours. False colours were defined for pixels above a given threshold in the total intensity image and below the maximum for pixels in the image, such that the surface composition is identified using one or more intensity ranges and colours. The image in Fig. 14 is visualised using six false-colours, representing the O 1s intensity map in a blue-red colour scale. The resulting colour scale allows the pixels of an image to be divided into areas of identical chemical state information identified by pixel colour and using the false colour image, as illustrated in Figures 15a-15f.

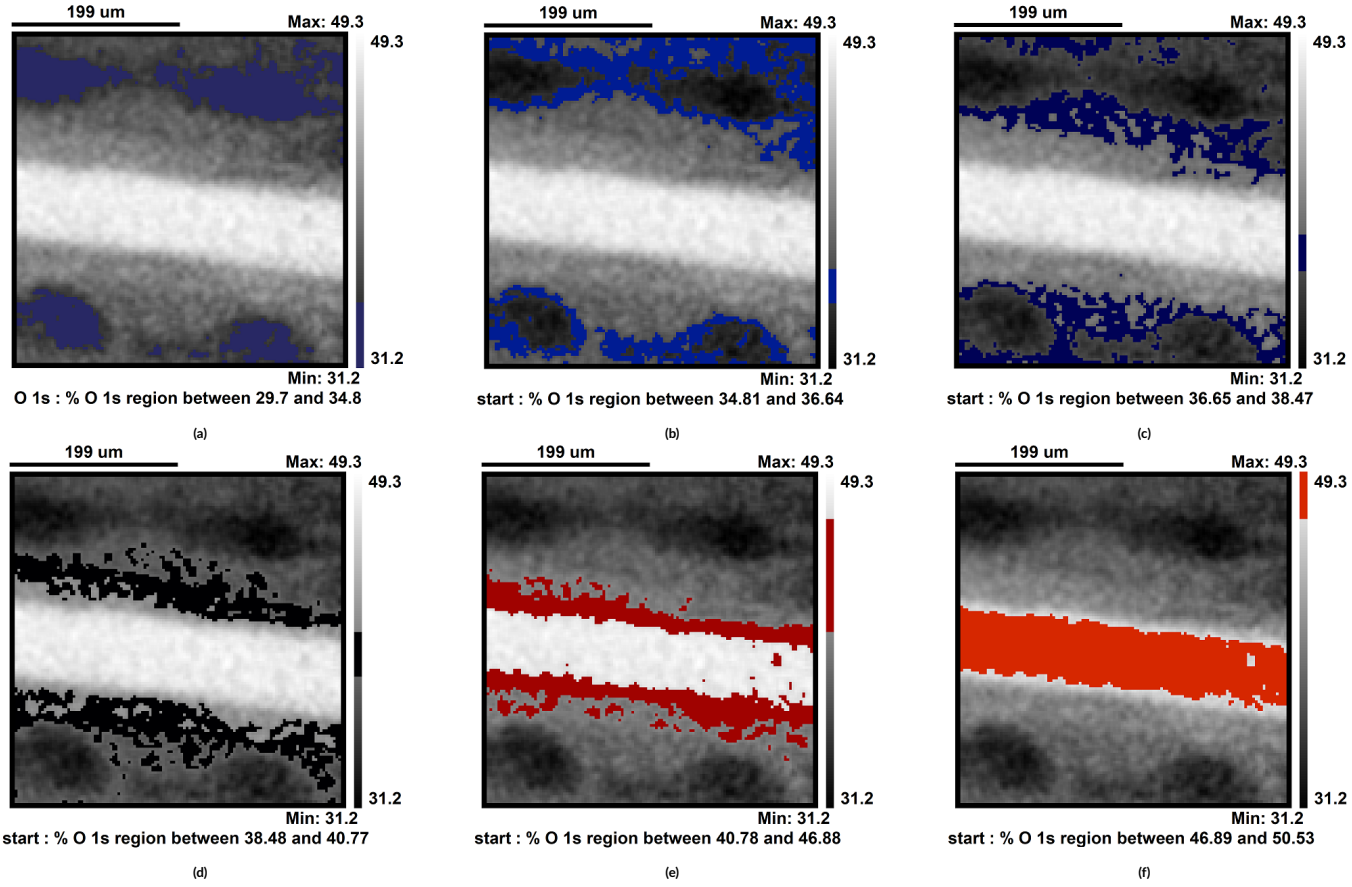

FIGURE 15 Set of images created by accumulating counts into pixels based on a false-colour-scale consisting of six colours corresponding to O 1s region between the atomic concentration interval values (a) 29.7% and 34.8%, (b) 34.81% and 36.64%, (c) 36.65% and 38.47%, (d) 38.48% and 40.77%, (e) 40.78% and 46.88%, and (f) 46.89% and 50.53%

associated to $C-O$ bonds is in accordance with the carbon contamination of the surface observed in figure 13[?]. The presence of oxygen in the trench, together with that of N and F, suggests either the formation of $Ti-O-N$ bonds on the surface of TiO_2 due to interstitial incorporation of nitrogen and /or the formation of $O-F_x$ compounds. The last suggestion can be excluded as no peak, in the O 1s core level spectrum, centred at about 535 eV was detected. Peak fitting allows the intensities attributed to these three chemical environments to be partitioned into separate

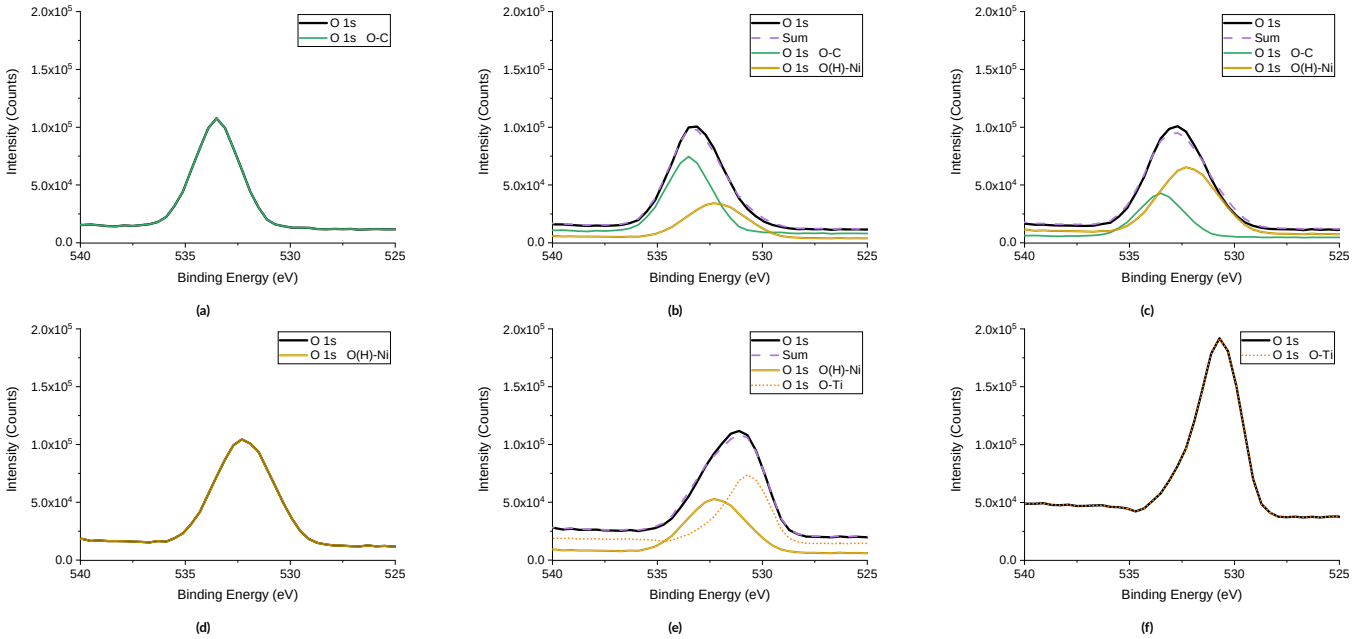

FIGURE 16 Spectra representing the sum of all the pixel spectra corresponding to each of the false-colours shown in Figure 15. Spectra summed from spectra at pixels for O 1s region between the interval values (a) 29.7%At. and 34.8%At., (b) between 34.81%At. and 36.64%At., (c) between 36.65%At. and 38.47%At., (d) between 38.48%At. and 40.77%At., (e) between 40.78%At. and 46.88%At., and (f) between 46.89%At. and 50.53%At.

images (Fig. 17), which when overlaid, support the spectral information in each pixel by reproducing images consistent with the expected result seen in Fig. 15.

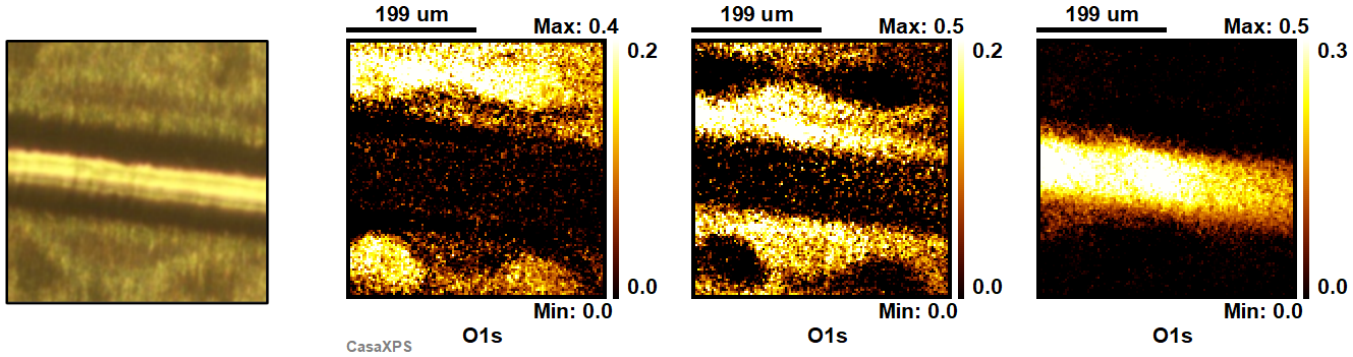

(a) Top view image of the 100 μm wide trench

(b) Binding Energy = 533.4 eV

Binding Energy = 532.3 eV

Binding Energy = 530.7 eV

FIGURE 17 Quantitative map with O 1s fit after peak-fitting spectra at each pixel using the model shown in Figure 14

The resulting chemical state maps (Fig. 17) revealed the spatial location of three different oxide species. The experimental variable for each of the images is the binding energy at which the image was acquired. The first image thus shows the organic C-O component, which can be corroborated by the C 1s map shown earlier; the second image corresponds to the hydroxyl compound and the hydroxidation of the mask on the surface. Finally, the last image confirms the oxidation of the titanium at the bottom of the trench. These latest findings show the importance of XPS imaging, combined with optical microscopy and EDS mapping, in the interpretation of the results. When etching titanium in a $Cl_2/SF_6/O_2$ mixture, and using a Ni mask, heavy contamination occurs on the mask surface. A low concentration of the elements F 1s and Cl 2p is identified, which suggests

the redeposition of etching products on the surface and in the surroundings of the trench, and which are visually recognisable by spots distributed on the mask. Furthermore, the oxidation of the mask and the titanium at the bottom of the trench is confirmed, which may indicate the passivating effect of oxygen in the $Cl_2/SF_6/O_2$ mixture. In some cases, the redeposition of etchants on the substrate is necessary so that the passivation layer that prevents lateral etching can form. However, this can also have detrimental effects, such as slowing down the etching rate or changing the shape of the etched profiles if the redeposition rate is too high or too low. Furthermore, in contrast to XPS imaging, EDS analyses did not allow the identification of the N lines, as these are almost overlapping with the Ti lines, another advantage of combining several analysis techniques.

4 | CONCLUSIONS

The aim of this work was to explore the innovative potential of the combined use of SEM+EDS and space resolved XPS techniques in surface analysis after plasma etching, as well as the emerging possibilities of imaging techniques. The results give a good overview of the contamination layers highlighting oxidation phenomena of both the mask and the titanium substrate, leading to the formation of a complex microchemical structure. From an analytical point of view, the results show that XPS imaging combined with optical microscopy can provide detailed information on the oxidation as well as the chemical nature of the surface. These results are consistent with the EDS chemical mapping performed after etching, which shows the presence of different O, C and Cl rich zones on the mask surface. XPS imaging on the same sample reveals three main oxygen environments. Thus, the ability of XPS imaging to map the chemical states of the elements provides greater accuracy in identifying the surface homogeneities of the sample. Furthermore, the results provide clear evidence of the interaction between inorganic constituents such as fluorine and chlorine in contact with the wafer during etching. An interesting insight towards these residues could be to identify the conditions and process parameters which are at the origin of these redeposits, or even to provide cleaning solutions compatible with the microfabrication process.

5 | ACKNOWLEDGMENTS

We thank the reviewers for their expert assistance with additional literature that helped the interpretation. The provided extensive feedback has improved the paper.

1. D'Agostino R, Fracassi F, Pacifico C. Dry etching of Ti in chlorine containing feeds. *J Appl Phys*. 1992; 72(9): 4351- 4357. https://doi.org/10.1063/1.352199

2. D'Agostino R, Fracassi F, Pacifico C, Capezzuto P. Plasma etching of Ti in fluorine-containing feeds. *J Appl Phys*. 1992; 71(1): 462- 471. https://doi.org/10.1063/1.350679

3. Aimi MF, Rao MP, MacDonald NC, Zuruzi AS, Bothman DP. High-aspect-ratio bulk micromachining of titanium. *Nature Mater*. 2004; 3(2): 103- 105.

4. Parker ER, Thibeault BJ, Aimi MF, Rao MP, MacDonald NC. Inductively coupled plasma etching of bulk titanium for MEMS applications. *J Electrochem Soc*. 2005; 152(10): C675- C683.

5. Parker ER, Thibeault BJ, Aimi MF, Rao MP, MacDonald NC. Monocyclic high aspect ratio titanium inductively coupled plasma deep etching processes and products so produced. US8685266B2, https://patents.google.com/patent/US8685266/en; 2014.

6. Rao MP, Aimit MF, Parker ER, MacDonald NC. Single-mask, high aspect ratio, 3-d micromachining of bulk titanium. In: IEEE International Conference on Micro Electro Mechanical Systems, MEMS. IEEE; 2005; Miami Beach, FL, USA: 64- 67.

7. Dussart R, Lefaucheux P, Tillocher T. Method for deep micro-etching. WO2013110583A1; 2013.

8. Tillocher T, Lefaucheux P, Boutaud B, Dussart R. Alternated process for the deep etching of titanium. *J Micromech Microeng*. 2014; 24(7):075021.

9. Fracassi F, D'Agostino R. Chemistry of titanium dry etching in fluorinated and chlorinated gases. *Pure Appl Chem*. 1992; 64(5): 703- 707.

10. Laudrel E, Tillocher T, Meric Y, Lefaucheux P, Boutaud B, Dussart R. The effect of SF_6 addition in a Cl_2 /Ar inductively coupled plasma for deep titanium etching. *J Micromech Microeng*. 2018; 28(5):055010.

11. Gott SC, Jabola BA, Guanshui, Xu, Rao MP. Vascular stents with rationally-designed surface patterning. In: 2012 Annual International Conference of the IEEE Engineering in Medicine and Biology Society. IEEE; 2012; San Diego, CA: 1639- 1642.

12. Gott SC, Jabola BA, Rao MP. Vascular stents with submicrometer-scale surface patterning realized via titanium deep reactive ion etching. *J Micromech Microeng*. 2015; 25(8):085016.

13. Khandan O, Kahook MY, Rao MP. Fenestrated microneedles for ocular drug delivery. *Sensors Actuators B Chem*. 2016; 223: 15- 23.

14. Parker ER, Rao M, Foster K, MacDonald NC. Bulk titanium microneedles with embedded microfluidic networks for transdermal drug delivery. In: IEEE International Conference on Micro Electro Mechanical Systems, MEMS; 2006: 498- 501.

15. Parker ER, Rao M, Foster K, Meinhart C, MacDonald NC. Bulk Micromachined Titanium Microneedles. *J Microelectromech Sys*. 2007; 16: 289- 295.

16. Grayson ACR, Shawgo RS, Johnson AM, Flynn NT, Li Y, Cima MJ, Langer R. A BioMEMS review: MEMS technology for physiologically integrated devices. *Proc IEEE*. 2004; 92(1): 6- 21.

17. Elias CN, Lima JHC, Valiev R, Meyers MA. Biomedical applications of titanium and its alloys. *Jom*. 2008; 60: 46- 49.

18. CXRO X-Ray Interactions With Matter. https://henke.lbl.gov/optical_constants/

19. Fairley N, Fernandez V, Richard Plouet M, et al. Systematic and collaborative approach to problem solving using X-ray photoelectron spectroscopy. *Appl Surf Sci Adv*. 2021; 5: 100112.

20. Goldstein JI, Newbury DE, Echlin P, et al. Scanning Electron Microscopy and X-ray Microanalysis. Boston, MA: Springer US; 2003(en). https://doi.org/10.1007/978-1-4615-0215-9

21. Biesinger MC, Payne BP, Lau LWM, Gerson A, Smart RSC. X-ray photoelectron spectroscopic chemical state quantification of mixed nickel metal, oxide and hydroxide systems. *Surf Interface Anal*. 2009; 41(4): 324- 332. https://doi.org/10.1002/sia.3026

22. El Mel AA, Angleraud B, Gautron E, Granier A, Tessier PY. XPS study of the surface composition modification of nc-TiC/C nanocomposite films under in situ argon ion bombardment. *Thin Solid Films*. 2011; 519(12): 3982- 3985.

23. Parra ER, Arango PJA, Palacio VJB. XPS structure analysis of TiN/TiC bilayers produced by pulsed vacuum arc discharge. *Dyna*. 2010; 77: 64- 74.

24. Biesinger MC, Lau LWM, Gerson AR, Smart RSC. The role of the Auger parameter in XPS studies of nickel metal, halides and oxides. *Phys Chem Chem Phys*. 2012; 14(7): 2434.

25. Grosvenor AP, Biesinger MC. New interpretations of XPS spectra of nickel metal and oxides. *Surf Sci*. 2006; 600: 1771- 1779.

26. Jolliffe IT, Cadima J. Principal component analysis: a review and recent developments. *Phil. Trans. R. Soc. A: Math Phys Eng Sci*. 2016; 374(2065):20150202. https://doi.org/10.1098/rsta.2015.0202

27. Malinowski ER, Howery DG. Factor analysis in chemistry, Vol. 3. New York: Wiley; 1980.

28. Walton J, Fairley N. XPS spectromicroscopy: exploiting the relationship between images and spectra. *Surf Interface Anal*. 2008; 40(3-4): 478- 481. https://doi.org/10.1002/sia.2731

29. Scofield JH. Hartree-Slater subshell photoionization cross-sections at 1254 and 1487 eV. *J Electron Spectrosc Relat Phenom*. 1976; 8(2): 129- 137.

30. Seah MP. Simple universal curve for the energy-dependent electron attenuation length for all materials. *Surf Interface Anal*. 2012; 44(10): 1353- 1359. https://doi.org/10.1002/sia.5033

31. Fakhouri H, Arefi-Khonsari F, Jaiswal AK, Pulpytel J. Enhanced visible light photoactivity and charge separation in TiO2/TiN bilayer thin films. *Appl Catal A: Gen*. 2015; 492: 83- 92.

32. Laidani N, Cheyssac P, Perrire J, Bartali R, Gottardi G, Luciu I, Micheli V. Intrinsic defects and their influence on the chemical and optical properties of TiO_x films. *J Phys D: Appl Phys*. 2010; 43(48):485402. https://doi.org/10.1088/0022-3727/43/48/485402